Available online at www.sciencedirect.com
SCIENCE DIRECT®
ELSEVIER
Journal of the European Ceramic Society 25 (2005) 1419–1429
ECERS
www.elsevier.com/locate/jeurceramsoc

# Microstructure and mechanical properties of $Al_2O_3$–YSZ and $Al_2O_3$–YAG directionally solidified eutectic plates

A. Larrea*, V.M. Orera, R.I. Merino, J.I. Peña

*Instituto de Ciencia de Materiales de Aragón, CSIC-Universidad de Zaragoza, E-50018 Zaragoza, Spain*

Available online 9 February 2005

**Abstract**

Plates of $Al_2O_3$–YSZ and $Al_2O_3$–YAG eutectic composition with a thickness from 0.1 to 1 mm were prepared by directional solidification using a diode laser stack. The melt processed regions of plates exhibited colony microstructure consisting of finely dispersed phases. Due to the curved shape of the melted pool, the growth rate depends on the distance to the surface plate, decreasing from top to bottom. In this way, the microstructure characteristic length changes as a function of the distance to the plate surface. Vickers indentations and piezo-spectroscopy measurements were done on longitudinal and transverse cross-sections of the samples at different depths. From these measurements, we concluded that the Vickers hardness ($H_V$), indentation fracture toughness ($K_{IC}$) and residual stresses ($\sigma_h$) of the plates were mainly independent from the distance to the surface. The mean values that we obtained in the $Al_2O_3$–YSZ plates were $H_V = 16$ GPa, $K_{IC} = 4.2$ MPa $m^{1/2}$ and $\sigma_h = -0.33$ GPa, and in the $Al_2O_3$–YAG plates were $H_V = 16$ GPa, $K_{IC} = 2.0$ MPa $m^{1/2}$, and $\sigma_h = -0.1$ GPa. These values are similar to those found in directionally solidified eutectic rods.


*Keywords:* Directionally solidified eutectics; Composites; Mechanical properties; $Al_2O_3$–$ZrO_2$; $Al_2O_3$–YAG

## 1. Introduction

Directionally solidified eutectics (DSE) contain a huge amount of clean interfaces between two strongly bonded phases with typical interphase spacing in the micron range. These characteristics result in an improvement of some material properties with respect to the properties of the constituent phases. In general, ceramic DSE materials are prepared in the form of melt grown rods or fibres. When the eutectic grows with ordered microstructure, like alternate lamellae or fibres in a matrix, some functional applications can be envisaged. For instance the $CaF_2$–MgO eutectic presents bunches of single-crystalline single-mode optical fibres with a density up to 40,000 pixel/$mm^2$.[1] Also the mixture of insulating and ionic conducting compounds as in the $CaZrO_3$–CaSZ (calcia stabilised zirconia) and MgO–MgSZ eutectics present a high anisotropic conductivity.[2] More recently it has been reported that porous CERMETs obtained after reduction of CoO and NiO–SZ lamellar eutectics exhibit both ionic and electronic conductivity and gas permeation properties suitable for solid oxide fuel cell anodes.[3] On the other hand, oxide–oxide eutectics besides their high chemical stability in oxidising atmospheres have excellent mechanical properties up to near the melting temperature.[4,5] For instance, rods of $Al_2O_3$–YSZ (yttria stabilised zirconia) and $Al_2O_3$–YAG (yttrium aluminium garnet) eutectics present a very high flexural and tensile strength and high toughness at room and high temperatures.[6,7]

Directionally solidified eutectics have been prepared in cylindrical geometry using different solidification procedures as Brigdman, floating zone melting, edge-defined film-fed growth or micro-pulling down methods. We recently reported the preparation of plates of $Al_2O_3$–$ZrO_2$ and NiO–CaSZ eutectics by laser zone surface melting and studied their microstructure.[8,3] By the same procedure we can now prepare sample areas of DSE material up to ~30 $cm^2$. Larger surface areas up to several $m^2$ could be processed using larger laser beams or overlapping adjacent laser scannings. These dense oxide–oxide eutectic plates display a smooth surface,

* Corresponding author.
*E-mail address:* alarrea@unizar.es (A. Larrea).

0955-2219/$ – see front matter © 2005 Elsevier Ltd. All rights reserved.
doi:10.1016/j.jeurceramsoc.2005.01.021

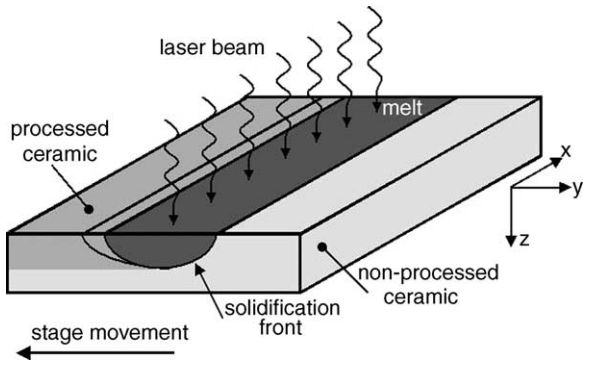


Fig. 1. Experimental set-up of the laser zone melting method showing a longitudinal cross-section of the processed plate.

and present high strength and toughness, chemical stability in oxidising environments as well as an excellent thermal shock resistance. They could be useful, for instance, as dense thermal barrier or anticorrosion coatings.

In this paper we describe the preparation and mechanical properties of $Al_2O_3$–YSZ and $Al_2O_3$–YAG directionally solidified eutectic plates. The absorbed laser radiation is used to increase the sample temperature and to melt the compound, as well as energy is transferred to the surrounding media by thermal diffusion and radiation dissipation processes. The steady state resultant from these processes determines the non-planar solidification front shape (Fig. 1), as described in Ref. 8. The solidification front curvature induces changes in both solidification direction and solidification rate as a function of the distance to the external surface, reflected in the eutectic microstructure. The solidification direction changes gradually from parallel to the external surface at the top of the processed layer to perpendicular to the surface at the bottom. Moreover, the solidification rate ($R$) gradually decreases from top to bottom, changing the interphase spacing ($\lambda$) which increases from top to bottom according to the $\lambda^2 R = \text{constant}$ equation.[9]

We have performed measurements of Vickers hardness ($H_V$), fracture toughness ($K_{IC}$) and residual stresses ($\sigma_h$) as a function of the depth and compared them with other results found in DSE rod samples. Hardness and fracture toughness are critical design parameters for structural applications of ceramic materials. The Vickers indentation method for calculating the fracture toughness of a material, although it could not be considered an accurate method for the absolute determination of the fracture toughness,[10] it is very convenient for comparative purposes. It is also very adequate in our case because it is a very simple and fast non-destructive analysis method. It is based on the measurement of real cracks and it requires a minimum quantity of the material to be analysed, providing $K_{IC}$ estimations in different points of the sample with spatial resolution. However, the measurement of the crack length is difficult and sometimes could be subjective. In addition, residual stresses can be measured along cross-sections of the sample with spatial resolution using piezo-spectroscopic techniques. The comparison between measured and calculated stresses gives information about the interface quality.

## 2. Experimental details

### 2.1. Sample preparation

Ceramic pellets (3 mm × 10 mm × 20 mm size) were produced by wet mixing of the $Al_2O_3$ (Aldrich 99.99%), $Y_2O_3$ (Aldrich 99.99%) and $ZrO_2$ (Aldrich 99%) starting powders. The mixture was moulded and subjected to uniaxial pressing up to 35 MPa followed by pressureless sintering 12 h at 1250 °C (heating rate 10 °C/min) plus 1 h at 1500 °C (heating rate 5 °C/min). The composition of the powder mixtures was: 63 mol% $Al_2O_3$ + 35.9 mol% $ZrO_2$ + 1.1 mol% $Y_2O_3$ for the $Al_2O_3$–YSZ eutectic and 80.9 mol% $Al_2O_3$ + 19.1 mol% $Y_2O_3$ for the $Al_2O_3$–YAG eutectic. After sintering the specimens had an approximate density of 3.3 g/cm$^3$ for the $Al_2O_3$–YSZ eutectic and 2.3 g/cm$^3$ for the $Al_2O_3$–YAG eutectic, i.e. approximately 70 and 55% of the theoretical density. Due to the high reflectance of the ceramic precursor some small amount, ∼1.5 mol%, of absorbing ions ($Co^{2+}$ or $Mn^{2+}$) were introduced in the starting powder to decrease the melting power threshold.

For the laser assisted directional solidification of plates the precursor pellets were supported on top of an $Al_2O_3$ dense plate that was moved at 500 mm/h speed under the static laser beam. The size of the laser spot, as is emerges from the commercial laser from Rofin Baasel ($\lambda$ = 810 nm, maximum power 600 W), was around 1 × 3.5 mm$^2$. We configured this beam by using cylindrical and spherical quartz lenses to form a spot of 1 × 12 mm$^2$. In Fig. 2 we show a photograph of one of the samples after the laser processing. Even if we start with a very inhomogeneous, rough and poor quality ceramic precursor we found that after processing the solidified zone is fairly homogeneous, displaying a smooth outer surface. The depth of the melted layer ranges from 100 to 1000 μm depending on the eutectic composition, laser power and processing speed. In the samples studied in the indentation and piezo-spectroscopic experi-

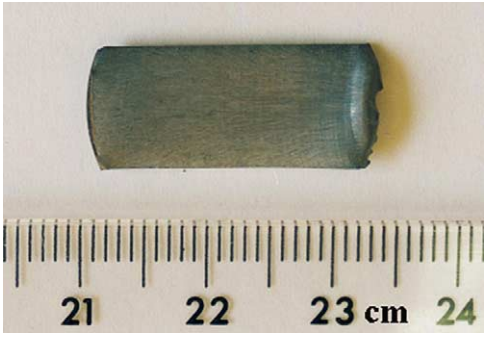


Fig. 2. Photograph of a laser processed plate. Solidification proceeds from left to right.

ments the depth of the melted layer was 560 μm in the case of $Al_2O_3$–YSZ plates (laser power 220 W) and 675 μm for $Al_2O_3$–YAG plates (laser power 155 W).

### 2.2. Characterisation

For the microstructure characterisation, Vickers indentations and piezo-spectroscopic measurements, transverse and longitudinal cross-sections (planes *XZ* and *YZ* of Fig. 1, respectively) were cut from the eutectic plates and embedded with epoxy resin. Then, these samples were grinded with SiC wet paper and polished with diamond paste down to 1/4 μm size. The microstructure of the samples was studied on carbon coated samples using a JEOL 6400 Scanning Electron Microscope (SEM) equipped with a Link Analytical X-ray detector for microanalysis experiments. Both Vickers hardness and fracture toughness were obtained from indentations made using a Matsuzawa MXT70 micro hardness tester and

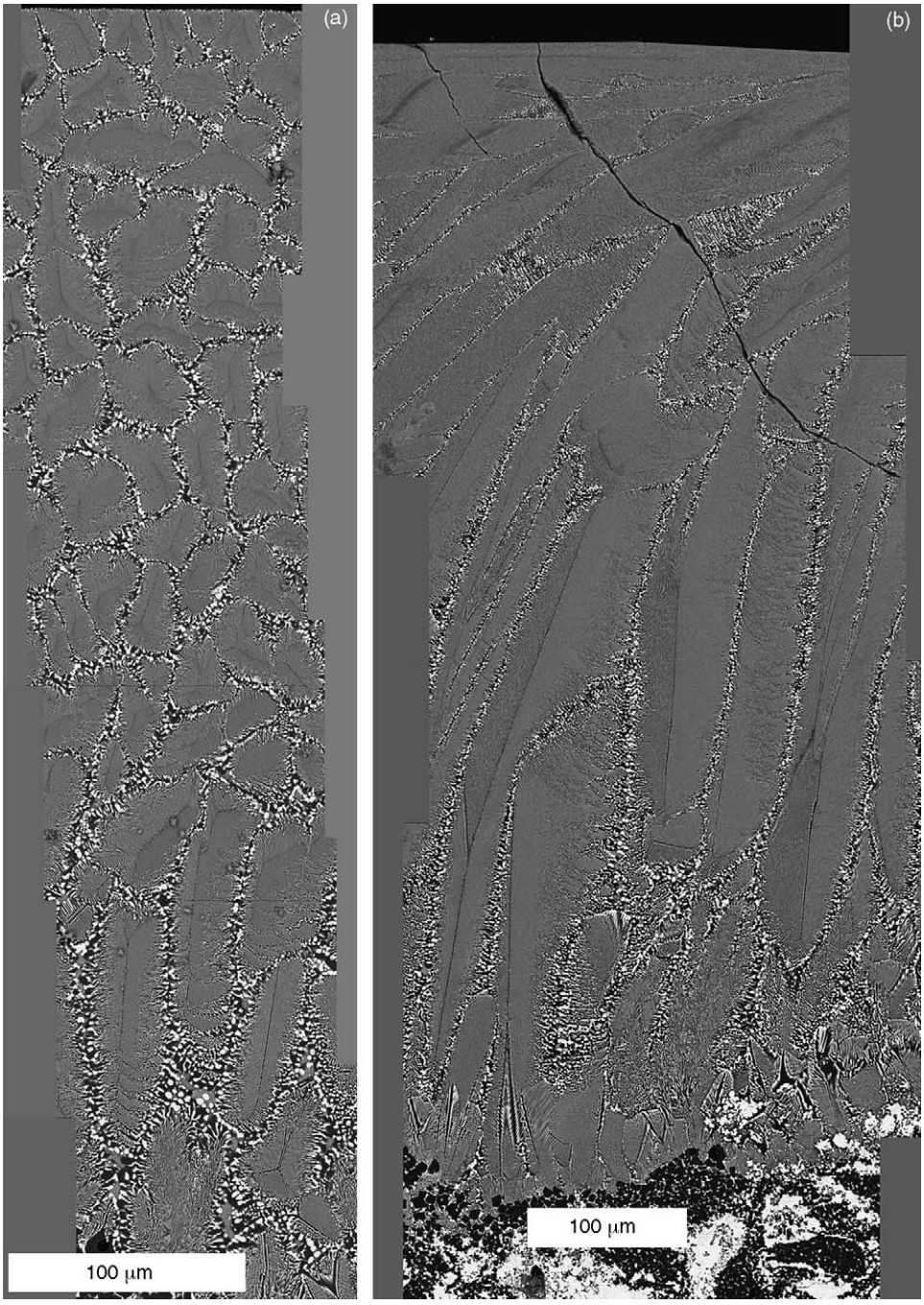


Fig. 3. SEM backscattered electron image of transverse (a) and longitudinal (b) cross-sections of the $Al_2O_3$–YSZ DSE plate. Light phase is YSZ and dark phase is $Al_2O_3$. Post-growth crack propagating perpendicularly to the colony axes (*c*-axis of the sapphire phase) can be observed in (b).

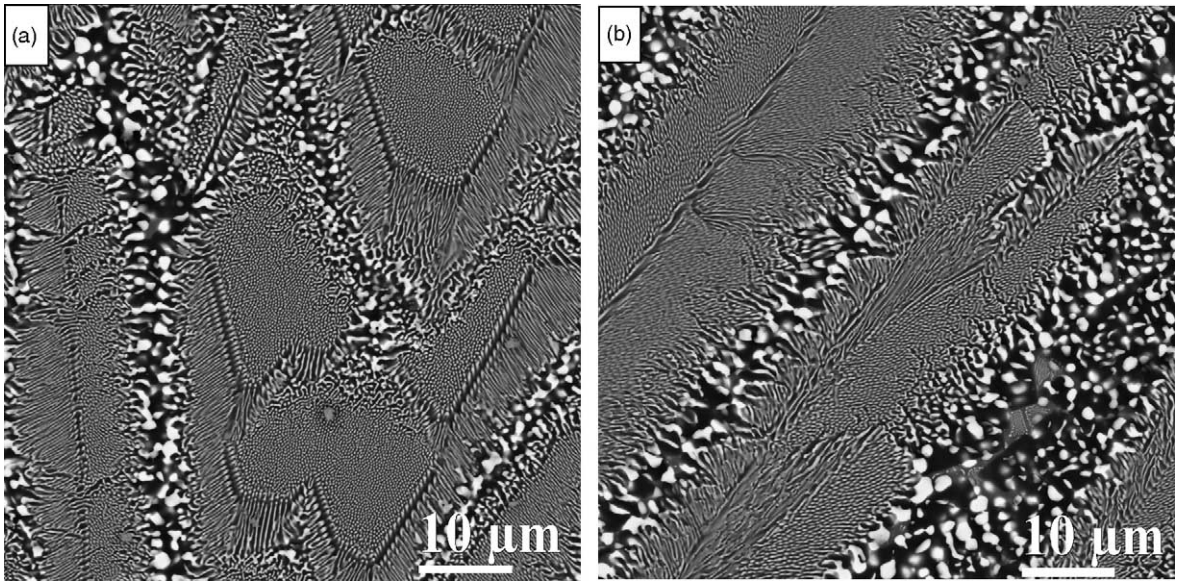


Fig. 4. Details of the transverse (a) and longitudinal (b) cross-sections in the central area of the $Al_2O_3$–YSZ DSE plate. Light phase is YSZ and dark phase is $Al_2O_3$.

9.81 N loads (15 s hold time). The quality of the polishing was previously checked in an optical microscope to be sure of the absence of scratches on the surfaces prior to indentation. The crack length and indentation diagonals were measured using the optical microscope and precision stage micrometer of the micro hardness tester. Special attention was paid to test the two eutectics studied in this work under the same experimental conditions. Micrographs of the cracks produced by the indentations were taken by SEM after coating the sample surface with a thin layer of Au by sputtering methods. The residual stresses in the $Al_2O_3$ phase of the eutectic plates were measured by means of the piezo-spectroscopic effect in the R-lines luminescence of $Cr^{3+}$ in $Al_2O_3$, whose maxima show a shift as a function of stress.[11,12] Traces of $Cr^{3+}$ impurity always present in commercial alumina powder were enough to allow spectroscopic measurements. These measurements were performed under backscattering geometry by means of an optical microprobe spectrometer with a diode array multichannel detector. Further details of the piezo-spectroscopic technique can be found elsewhere.[13,14]

## 3. Experimental results and discussion

### 3.1. Microstructure

The microstructure of the $Al_2O_3$–YSZ plates is formed by elongated colonies (Figs. 3 and 4). In Laser Floating Zone $Al_2O_3$–YSZ grown rods showing the same microstructure,[15,16] it has been proposed that eutectic growth is driven by the crystallisation of $Al_2O_3$, very often with the R crystallographic planes forming facets, and a hexagonal pattern of $ZrO_2$ fibres embedded into those crystals. With this kind of microstructure, the size, shape and orientation of the colonies, the interphase spacing inside the colonies and also the width of the intercolony region are the relevant magnitudes. The diameter of the colonies (shortest width, parallel to the surface, in the transverse cross-section) has almost no dependence on the depth from the surface. On the contrary, the orientation of the colonies (long axis of the colony) and the width of the intercolony region are dependent on the $z$ coordinate. Average colony diameter is around 21 μm. A plot of the interphase and intercolony spacing as a function of depth seems to show a variation. The interphase spacing changes from $\lambda \sim 0.3$ μm in the top of the plate to $\lambda \sim 1$ μm in the bottom. The intercolony spacing ranges from around 3 μm at the surface and half of the sample thickness to approximately 11 μm near to the unprocessed ceramic, always with large dispersion. In the intercolony region pores and secondary phases involving the doping ions occasionally appear, as determined by Energy Dispersive Spectroscopy microanalysis. The determination of the orientation of the colony axis has been obtained from longitudinal cross-sections. Colonies always grow perpendicular to the solidification front. However, since the growth of the colonies is driven to a large extent by crystallography, and its length is not small compared to the length scale of the melt depth, large deviations of a particular colony orientation to the one imposed by the thermal gradient are expected and observed.

The longitudinal and transverse cross-sections of the microstructure for the directionally solidified $Al_2O_3$–YAG are shown in Figs. 5 and 6, respectively. Colonies are observed all over the plates. The kind of Chinese Script microstructure, usually found in this eutectic,[17,18] and characterised by jagged interfaces between the component phases, is also observed here. The size of the colonies is around 22 μm, and similarly to the previously described $Al_2O_3$–YSZ eutectic the interphase and intercolony spacings increases from the sur-

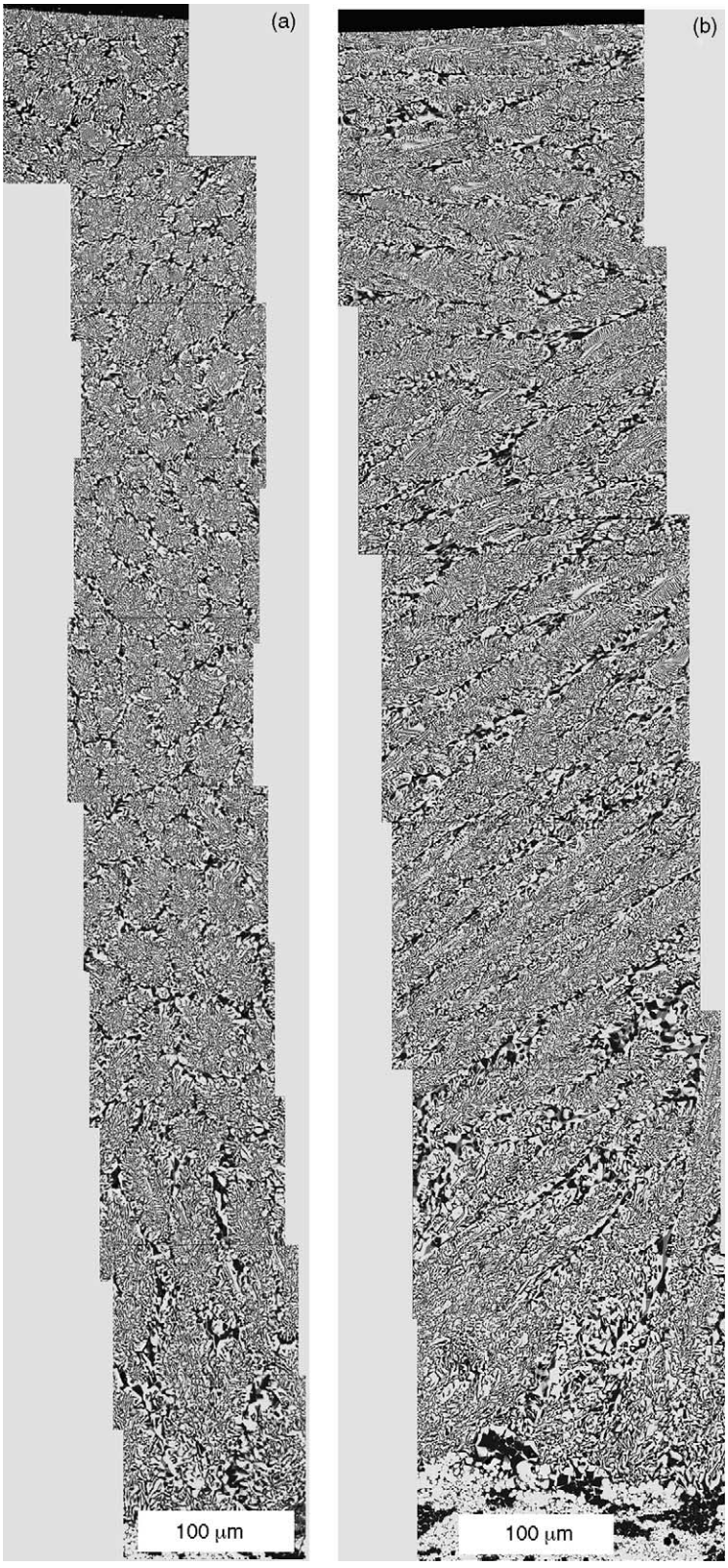


Fig. 5. SEM backscattered electron image of transverse (a) and longitudinal (b) cross-sections of the $Al_2O_3$–YAG DSE plate. Light phase is YAG, dark phase is $Al_2O_3$.

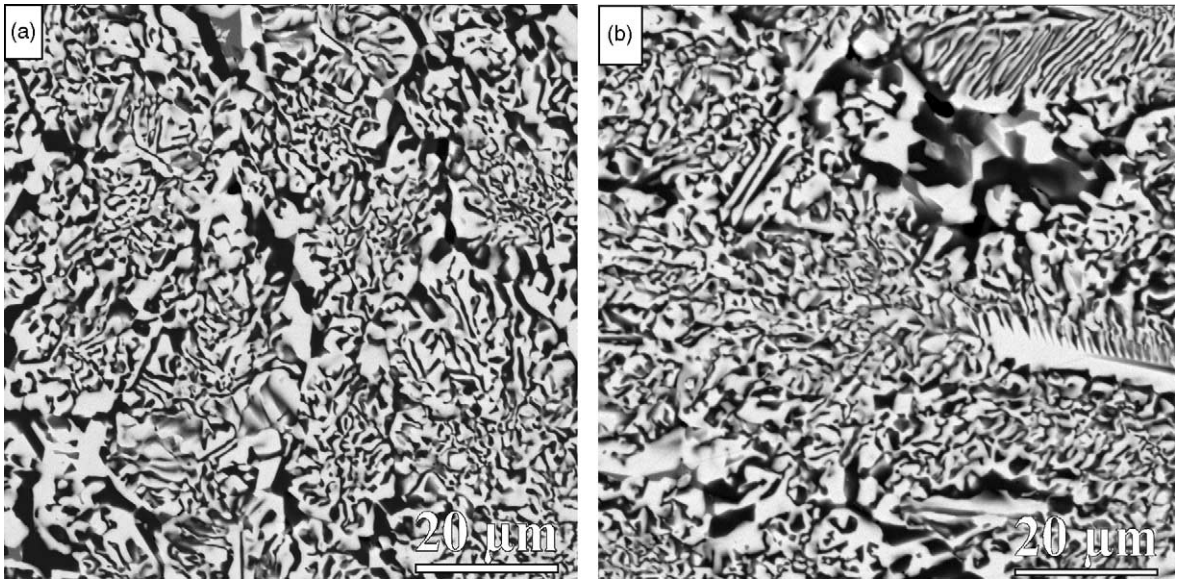


Fig. 6. Details of the transverse (a) and longitudinal (b) cross-sections in the central area of the $Al_2O_3$–YAG DSE plate. Light phase is YAG and dark phase is $Al_2O_3$.

face towards the unprocessed ceramic. The interphase spacing ranges from $\lambda \sim 0.5\,\mu m$ at the top of the plate to $\lambda \sim 2\,\mu m$ at the bottom. The intercolony region thickness takes values of 4 μm in average near to the surface and around 12 μm near the unprocessed ceramic side, always with large dispersion. As in the case of $Al_2O_3$–YSZ plates, colonies nucleate approximately perpendicular to the unprocessed ceramic at the bottom of the processed layer but run parallel to the surface in the outer end of the layer.

### 3.2. Residual stresses

Due to the differences in thermal expansion coefficients of the $Al_2O_3$–YSZ component phases, thermoelastic stresses develop during the cool down process. We measured the residual stresses in the $Al_2O_3$ phase by means of the piezospectroscopic effect of the ruby R emission lines. The $R_1$ and $R_2$ luminescence lines of $Cr^{3+}$ ions in alumina appear at approximately 14,405 and 14,435 $cm^{-1}$ in an unstressed ruby at room temperature and their positions change with stress. This behaviour can be used to calculate the residual stresses in the alumina phase from the values of the piezospectroscopic tensors, $\Pi_{ij}$, as determined by He and Clarke.[19] They are diagonal with respect to the ruby crystallographic axes. Assuming that the piezo-spectroscopic effect is isotropic in the alumina basal plane, $\Pi_{11} \approx \Pi_{22}$, the peak shift $\Delta\nu$ between the stressed and unstressed ruby is given for the two $R_1$ and $R_2$ lines by:

$$\Delta\nu_1 = 3.26(\sigma_{11} + \sigma_{22}) + 1.53\sigma_{33} \quad (1a)$$

$$\Delta\nu_2 = 2.73(\sigma_{11} + \sigma_{22}) + 2.16\sigma_{33} \quad (1b)$$

where $\sigma_{ii}$ ($i = 1, 2, 3$) stand for stress components along the *a*-, *m*- and *c*-axes of the hexagonal sapphire lattice, respectively. The hydrostatic stress is defined by $\sigma_h = (\sigma_{11} + \sigma_{22} + \sigma_{33})$. A negative value means compression stress whereas positive values stand for tensile stresses.

We measured the luminescence $R_1$ and $R_2$ lines along the plate depth in a transverse section and compared with those of unstressed ruby in the same experimental conditions. In Fig. 7 we give the hydrostatic stress values calculated from the shifts in peak positions $\Delta\nu_1$ and $\Delta\nu_2$ of the R-lines relative to these of unstressed ruby and using Eqs. (1a) and (1b). It should be noticed that we obtained average stress values because the piezospectroscopic measurements were done in areas larger than the microstructural characteristic size. In agreement with previous studies in rod-like samples for this composition the alumina phase is under compression stress.[20] The hydrostatic residual stress take a value of $\sigma_h = -0.4 \pm 0.1$ GPa near to the surface and smoothly diminish to $\sigma_h = -0.3 \pm 0.1$ GPa near to the ceramic, decreasing abruptly to zero stress in the melt-ceramic interface.

The stress components in the zirconia phase can be evaluated from the static equilibrium condition as

$$f^A\sigma_{ii}^A + f^Z\sigma_{ii}^Z = 0, \quad \forall i = 1, 2, 3 \quad (2)$$

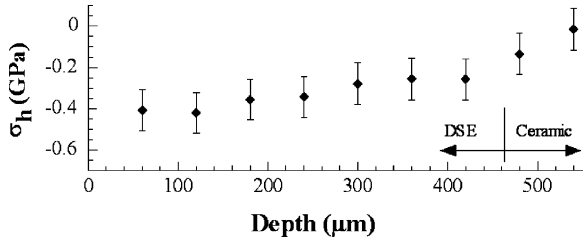


Fig. 7. Hydrostatic residual stresses in the $Al_2O_3$ phase measured on the transverse cross-section of an $Al_2O_3$–YSZ eutectic plate as a function of the distance to the surface.

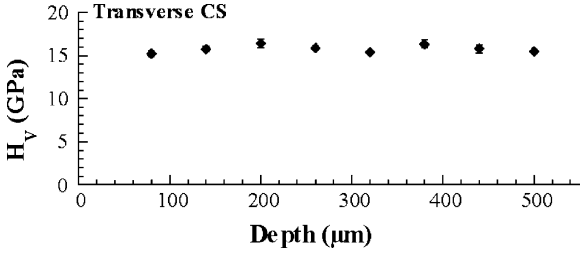


Fig. 8. Vickers hardness measured on the transverse cross-section of an $Al_2O_3$–YSZ eutectic plate as a function of the distance to the surface.

where $f^A$ (=0.7) and $f^Z$ (=0.3) stand, respectively, for the volume fraction of alumina (A) and zirconia (Z). In consequence zirconia phase is under tensile stress.

The residual stress value for this sample coincides with that obtained in rod-like samples of the same composition. They also agree with residual stress calculations based on self-consistent methods.[13] Absence of any residual stress relaxation indicate that the interfaces are strong.

On the other hand, the $Al_2O_3$–YAG eutectic is very different from the $Al_2O_3$–YSZ eutectic with regard to residual stresses. There is not significant mismatch between the coefficients of thermal expansion of the constituent phases and no relevant residual stresses are developed upon cooling.[21] In our case the hydrostatic stress is also constant through the plate and takes a value of $\sigma_h = -100 \pm 50$ MPa in the alumina phase.

### 3.3. Vickers hardness and fracture toughness

In-depth measurements of Vickers hardness and fracture toughness were done on both transverse and longitudinal cross-sections by the indentation fracture method for the two eutectics studied in this work. Each data point corresponds to the average of two indentations performed following the recommendations of ASTM C1327-99 document[22] concerning the closest permitted spacing for Vickers indentations. Fig. 8 shows, as a representative example, the measurements of Vickers hardness done in the transverse cross-section of the $Al_2O_3$–YSZ eutectic plate. Lee et al. reported that hardness increases as the microstructure become finer in $Al_2O_3$–$ZrO_2$ fibres produced by the micro-pulling down method.[23] Vickers hardness, however, is constant through both the transverse and longitudinal cross-sections samples for the two eutectics reported in this work. The average results are compiled in Table 1. Our results are also similar to those previously reported for eutectics of the same composition but grown by different methods. Hence, Pastor et al.[6] reported for $Al_2O_3$–YSZ (9 mol% $Y_2O_3$) rods (Ø 1.3–2.2 mm) grown by the laser floating zone method a Vickers hardness of $15.3 \pm 0.2$ GPa and $14.6 \pm 0.1$ GPa measured on transverse and longitudinal cross-sections respectively. Echigoya et al.[24] studied the Vickers hardness as a function of the $Y_2O_3$ content also in rod-like samples directionally solidified in an infrared heating furnace. They reported a maximum of $H_V = 16.7$ GPa for the 3 mol% $Y_2O_3$ composition and a value of $H_V = 14.7$ GPa for the 13 mol% $Y_2O_3$ composition. Borodin et al.[25] in $Al_2O_3$–YSZ (5.3 mol% $Y_2O_3$) DSE rods with colony microstructure produced by the Stepanov technique found a value of $H_V = 16.7$ GPa. Yang et al.[26] used the indentation method for fracture toughness measurements in $Al_2O_3$–YAG eutectics fibres prepared by edge-defined film-fed growth (Ø 125 μm). Although they did not report the Vickers hardness it is possible to estimate it from the micrographs to be about 16 GPa. All these results suggest that the Vickers hardness of $Al_2O_3$–YSZ and $Al_2O_3$–YAG eutectics is mainly dominated by the hardness of $Al_2O_3$ ($Al_2O_3$: $H_V = 14.7$–$16.2$ GPa; YSZ: $H_V = 12.3$ GPa; YAG: $H_V = 13.7$ GPa), with no marked dependence on the eutectic microstructure or growth method.

Table 1
Mean Vickers hardness measured on transverse and longitudinal cross-sections of the eutectic plates

| | $Al_2O_3$–YSZ (GPa) | $Al_2O_3$–YAG (GPa) |
|---|---|---|
| CS-transverse | 15.7 (0.5) | 16.1 (0.3) |
| CS-longitudinal | 16.3 (0.4) | 15.9 (0.6) |

The standard deviation is indicated between parentheses.

To account for the possible influence of the anisotropy of the microstructure $K_{IC}$ was calculated separately from cracks propagating either parallel or perpendicular to the plate surface. For each data point we measured four crack lengths from to the two indentations made at each depth. In this way we obtained the average length and its standard deviation for parallel and perpendicular crack propagation. Different approaches were considered for the two composites to derive the fracture toughness from these raw data. It has been previously verified[6,24] that cracks produced by indentations in $Al_2O_3$–YSZ melt grown composites are Palmqvist type, so the calculation of $K_{IC}$ was made using the equation proposed by Niihara et al.[27] for Palmqvist type cracks:

$$K_{IC} = 0.035\left(\frac{H}{E}\right)^{-\frac{2}{5}}\left(\frac{l}{a}\right)^{-\frac{1}{2}} H a^{\frac{1}{2}} \phi^{-\frac{3}{5}} \quad (3)$$

where $E$ is the Young's Modulus of the material (we have taken the value of $343 \pm 7$ GPa measured by Pastor et al.[6] for the same eutectic), $H$ is the Vickers hardness, $l$ is the crack length, $a$ is half the indentation diagonal and $\phi \simeq 3$ is a constrain factor. We have also verified by polishing the indented surface that the cracks produced in the plates were Palmqvist type. Moreover, in our case $l \simeq 12$–$18$ μm (depending on the propagation direction: $X$, $Y$ or $Z$ directions of Fig. 1) and $\phi \simeq 17$ μm, so the $0 \leq l/a \leq 2.5$ Niihara condition for Palmqvist cracks is fulfilled. A SEM micrograph displaying the cracking pattern nucleated at the corners of a Vickers indentation is shown in Fig. 9. Elastic ligaments between the cracks are often observed as it has been previously reported in DSE rods of the same composition.[6]

We show in Fig. 10 the fracture toughness measured in $Al_2O_3$–YSZ eutectic plates as a function of the distance to the surface plate. The results are reported separately for cracks

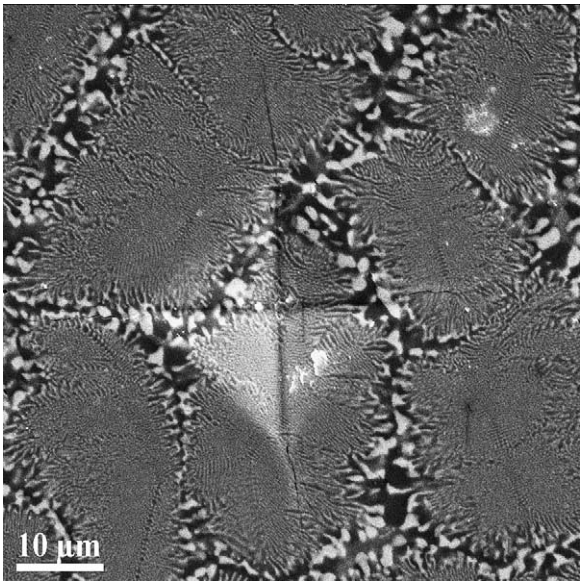


Fig. 9. Indentation on an $Al_2O_3$–YSZ eutectic plate transverse cross-section with cracks emerging from the corners.

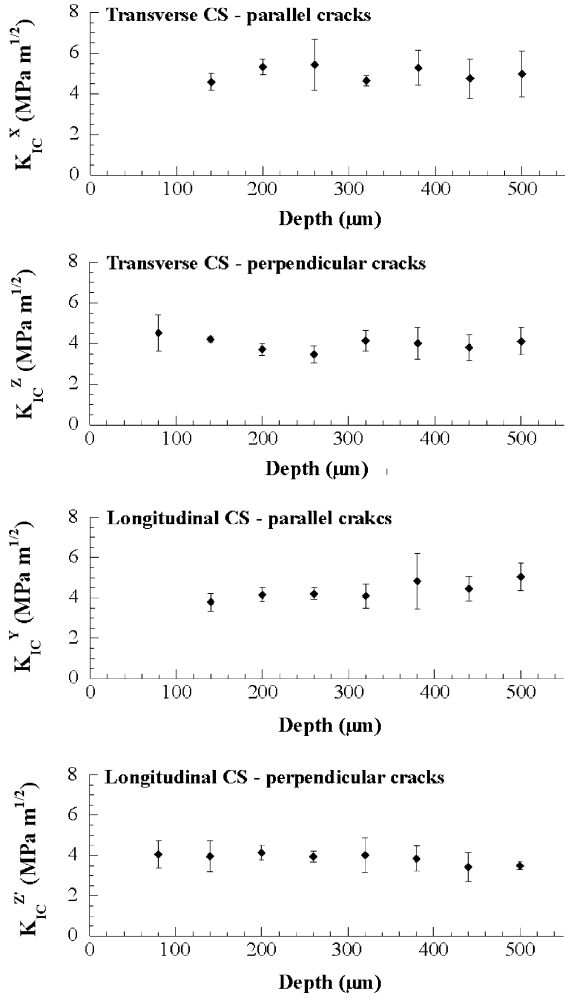


Fig. 10. Fracture toughness of the $Al_2O_3$–YSZ eutectic plate measured on longitudinal and transverse cross-sections from cracks propagating parallel and perpendicular to the plate surface. The directions corresponding to those depicted in Fig. 1 are indicated as a superscript.

propagating parallel or perpendicular to the surface on transverse and longitudinal cross-sections. It can be observed that fracture toughness is mainly independent of the distance to the surface. The nearest to surface measurements corresponding to cracks parallel to the surface were discarded because they were in the limit of closest allowable distance to the surface to make indentations with 9.81 N loads.

The average values are represented in Table 2. The four data reported correspond to three directions in the space. Cracks parallel to the surface in the transverse and longitudinal cross-sections correspond respectively to cracks propagating in the *X* and *Y* directions of Fig. 1. Cracks perpendicular to the surface in the transverse and longitudinal cross-sections both correspond to cracks propagating in the *Z* direction of Fig. 1. Note that the mean fracture toughness calculated from perpendicular cracks on the transverse and longitudinal cross-sections are nicely coincident. Although the data have high standard deviations, some anisotropy could be deduced from the experiments: $K_{IC}^{Z} < K_{IC}^{Y} < K_{IC}^{X}$. This anisotropy might be related to different relative orientation of the cracks with respect to the colony axes and intercolony regions as can be observed in Fig. 3.

With respect to the comparison of our results with those given the literature, Borodin et al.[25] found a mean value of about 5.6 MPa $m^{1/2}$ in $Al_2O_3$–YSZ (5.3 mol% $Y_2O_3$) DSE rods with colony microstructure, Echigoya et al.,[24] using the indentation method on fibrous $Al_2O_3$–YSZ DSE, obtained values of $K_{IC}$ from 8 to 4 MPa $m^{1/2}$ depending on the $Y_2O_3$ content. Nevertheless, Pastor et al.[6] found by the indentation method very similar values of fracture toughness, $K_{IC} \sim 5$ MPa $m^{1/2}$, on $Al_2O_3$–YSZ DSE rods with colony microstructure. They also reported in the same samples a "true" value of $K_{IC} = 7.8 \pm 0.3$ MPa $m^{1/2}$ obtained by fracture tests in notched rods.

In the $Al_2O_3$–YAG plates we verified, by polishing the indented surface, that cracks produced by $P = 9.81$ N indentations are median type cracks and in consequence we used a different approach to calculate $K_{IC}$. The equation proposed

Table 2
Mean fracture toughness measured on transverse and longitudinal cross-sections of $Al_2O_3$–YSZ eutectic plates

| $Al_2O_3$-YSZ | Parallel cracks (MPa $m^{1/2}$) | Perpendicular cracks (MPa $m^{1/2}$) |
|---|---|---|
| CS-transverse | $K_{IC}^{X} = 4.77\,(0.74)$ | $K_{IC}^{Z} = 3.96\,(0.33)$ |
| CS-longitudinal | $K_{IC}^{Y} = 4.37\,(0.44)$ | $K_{IC}^{Z'} = 3.86\,(0.26)$ |

The standard deviation is indicated between parentheses.

Table 3
Mean fracture toughness measured on transverse and longitudinal cross-sections of $Al_2O_3$–YAG eutectic plates

| $Al_2O_3$–YAG | Parallel cracks (MPa $m^{1/2}$) | Perpendicular crack (MPa $m^{1/2}$) |
|---|---|---|
| CS-transverse | $K_{IC}^{X} = 2.01\,(0.14)$ | $K_{IC}^{Z} = 2.07\,(0.31)$ |
| CS-longitudinal | $K_{IC}^{Y} = 2.05\,(0.20)$ | $K_{IC}^{Z'} = 1.89\,(0.17)$ |

The standard deviation is indicated between parentheses.

by Anstis[28] for these cracks is:

$$K_{IC} = 0.016\left(\frac{E}{H}\right)^{\frac{1}{2}}\left(\frac{P}{C^{\frac{3}{2}}}\right) \quad (4)$$

where $P$ is the indentation load, $c$ is the distance from the centre of the indentation to the crack tip and $E = 330 \pm 5$ GPa is the value measured by J.Y. Pastor in $Al_2O_3$–YAG DSE samples.[29] Since in our case $c \simeq 50$ μm and $a \simeq 17$ μm, the crack lengths also fulfilled the Niihara condition for median cracks: $c/a \geq 2.5$.[27] It should be pointed out, however, that Park and Yang[30] reported the formation of Palmqvist type cracks in $Al_2O_3$–YAG eutectic fibres using 100 g loads. This result, nevertheless, does not disagree with our results because it has been experimentally determined that Palmqvist cracks are formed when the load is not high enough to produce median cracks.[10]

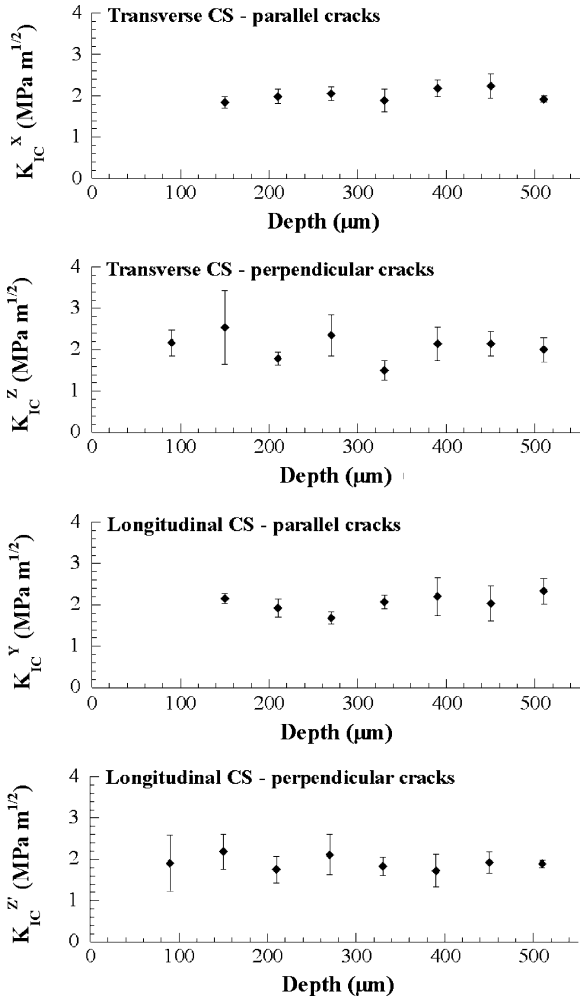


Fig. 11. Fracture toughness of the $Al_2O_3$–YAG eutectic plate measured on longitudinal and transverse cross-sections from cracks propagating parallel and perpendicular to the plate surface. The directions corresponding to those depicted in Fig. 1 are indicated as a superscript.

Fracture toughness values for $Al_2O_3$–YAG eutectic plates as a function of the distance to the surface is shown in Fig. 11. As in the preceding case we have calculated $K_{IC}$ from cracks propagating either perpendicular or parallel to the surface of transverse and longitudinal cross-sections. Fracture toughness is also constant through the sample and no anisotropy is observed in crack propagation (Table 3). Contrary to the former $Al_2O_3$–YSZ case where some fracture toughness anisotropy was observed, the microstructure of the $Al_2O_3$–YAG plates does not displays such an evident microstructural anisotropy as can be observed in Fig. 5.

Our $Al_2O_3$–YAG results can be compared with those given by other authors. Yang et al.[26] reported for DSE thin fibres (125 μm diameter) values of $K_{IC} = 2.0$ MPa $m^{1/2}$ and $K_{IC} = 2.4$ MPa $m^{1/2}$ obtained by the indentation method in directions parallel and perpendicular to the fibre axis, although they used for its calculations an unrealistic value of $E = 400$ GPa. Ochiai et al., using three-point bending tests to study 3 mm × 4 mm × 40 mm ingots cut from DSE rods produced by high frequency induction-heating, found values of $K_{IC}$ around 2–4 MPa $m^{1/2}$ in the temperature range of RT to 2000 K.[31]

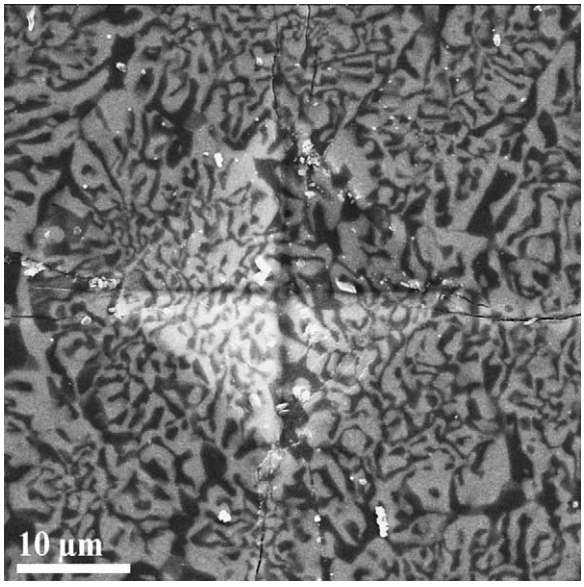


Fig. 12. Indentation on an $Al_2O_3$–YAG eutectic plate transverse cross-section with cracks emerging from the corners.

A micrograph showing the cracking pattern in $Al_2O_3$–YAG plates can be observed in Fig. 12. Multiple cracks are generally formed at the indentation corners. These cracks are usually 5–12 μm length until one of them became dominant and propagates in a near straight line around 33 μm length. Interfaces do not deflect cracks probably because they are very strong. In contrast to the former $Al_2O_3$–YSZ case no bridging effects are observed in crack propagation.

## 4. Summary

The preparation of large area plates of $Al_2O_3$–YSZ and $Al_2O_3$–YAG DSE is reported. These materials are characterised by a colony microstructure where, due to the curvature of the solidification front, the orientation of the colonies, as well as the interphase spacing gradually change in the melted plates from the top of the processed layer to the bottom near the unprocessed ceramic. In both $Al_2O_3$–YSZ and $Al_2O_3$–YAG plates the thickness of the intercolony region goes from approximately 3 μm at the surface to around 11 μm near to the ceramic precursor. However, the mechanical properties we have characterised (residual stress, Vickers hardness and fracture toughness) are approximately constant through the plate depth. Moreover, we have obtained for these properties similar values than the previously reported in DSE rods of the same composition. We have also found some anisotropy (22%) in the mean fracture toughness of $Al_2O_3$–YSZ plates with respect the transverse and perpendicular axes of the plate, whereas no such anisotropy has been found in $Al_2O_3$–YAG plates.

## Acknowledgements

Financial support from the Spanish Ministry of Science and Technology through projects MAT2000-1495 and MAT2003-06085-C03-01 is acknowledged. Fruitful discussions with J.Y. Pastor are kindly acknowledged.

## References

1. Larrea, A., Contreras, L., Merino, R. I., Llorca, J. and Orera, V. M., Microstructure and physical properties of $CaF_2$–MgO eutectics produced by the Bridgman method. *J. Mater. Res.*, 2000, **15**, 1314–1319.
2. Merino, R. I., Peña, J. I., Orera, V. M. and de la Fuente, G. F., Conductivity anisotropy in directionally solidified $CaZrO_3$–CaSZ and MgO–MgSZ eutectics. *Solid State Ionics*, 1997, **100**, 313–318.
3. Merino, R. I., Peña, J. I., Laguna-Bercero, M. A., Larrea, A. and Orera, V. M., Directionally solidified calcia stabilised zirconia-nickel oxide plates in anode supported SOFC's. *J. Europ. Ceram. Soc.*, 2004, **24**, 1349–1353.
4. Sayir, A., Farmer, S. C., Dickerson, P. O. and Yun, H. M., High temperature mechanical properties of $Al_2O_3/ZrO_2(Y_2O_3)$ fibers. *Mat. Res. Soc. Symp. Proc.*, 1995, **365**, 21–27.
5. Mazerolles, L., Michel, D. and Pérez y Jorba, M., Microstructure and related properties of oriented eutectics involving refractory oxides. In *Studies in Inorganic Chemistry, Vol 3*, ed. R. Metselaar, H. J. M. Heijligers and J. Schoonman. Elsevier, Amsterdam, 1984, pp. 841–844.
6. Pastor, J. Y., Poza, P., LLorca, J., Peña, J. I., Merino, R. I. and Orera, V. M., Mechanical properties of directionally solidified $Al_2O_3$–$ZrO_2(Y_2O_3)$ eutectics. *Mater. Sci. Eng.*, 2001, **A308**, 241–249.
7. Mah, T., Parthasarathy, T. A. and Matson, L. E., Processing and mechanical properties of $Al_2O_3/Y_3Al_5O_{12}$ (YAG) eutectic composite. *Ceram. Eng. Sci. Proc.*, 1990, **11**, 1617–1627.
8. Larrea, A., de la Fuente, G. F., Merino, R. I. and Orera, V. M., $ZrO_2$-$Al_2O_3$ eutectic plates produced by laser zone melting. *J. Europ. Ceram. Soc.*, 2002, **22**, 191–198.
9. Chalmers, B., *Principles of Solidification*. John Wiley and Sons, New York, 1964.
10. Pastor, J.Y., *Fractura de Materiales Cerámicos Estructurales Avanzados*. Ph.D. thesis, Universidad Complutense de Madrid, Madrid, Spain, 1993.
11. He, J. and Clarke, D. R., Determination of the piezospectroscopic coefficients for chromium-doped sapphire. *J. Am. Ceram. Soc.*, 1995, **78**, 1347–1350.
12. He, J. and Clarke, D. R., Determination of fiber strength distributions from bundle tests using optical luminescence spectroscopy. *Proc. R. Soc. Lond.*, 1997, **A453**, 1881–1901.
13. Pardo, J. A., Merino, R. I., Orera, V. M., Peña, J. I., González, C., Pastor, J. Y. and LLorca, J., Piezospectroscopic study of residual stresses in $Al_2O_3$–$ZrO_2$ directionally solidified eutectics. *J. Am. Ceram. Soc.*, 2000, **83**, 2745–2752.
14. Orera, V. M., Cemborain, R., Merino, R. I., Peña, J. I. and Larrea, A., Piezo-spectroscopy at low temperatures: residual stresses in $Al_2O_3$–$ZrO_2(Y_2O_3)$ eutectics measured from 77 to 350 K. *Acta Mater.*, 2002, **50**, 4677–4686.
15. Peña, J. I., Merino, R. I., Harlan, N. R., Larrea, A., de la Fuente, G. F. and Orera, V. M., Microstructure of $Y_2O_3$ doped $Al_2O_3$–$ZrO_2$ eutectics grown by the laser floating zone method. *J. Europ. Ceram. Soc.*, 2002, **22**, 2595–2602.
16. Farmer, S. C. and Sayir, A., Tensile strength and microstructure of $Al_2O_3$–$ZrO_2$ hypo-eutectic fibers. *Eng. Fract. Mechan.*, 2002, **69**, 1015–1024.
17. Mah, T., Parthasarathy, T. A., Petry, M. D. and Matson, L. E., Processing, microstructure, and properties of $Al_2O_3/Y_3Al_5O_{12}$ (YAG) eutectic fibers. *Ceram. Eng. Sci. Proc.*, 1993, **14**, 622–638.
18. Frazer, C. S., Dickey, E. S. and Sayir, A., Crystallographic texture and orientation variants in $Al_2O_3/Y_3Al_5O_{12}$ directionally solidified eutectic crystals. *J. Cryst. Growth*, 2001, **233**, 187–195.
19. He, J. and Clarke, D. R., Polarization dependence of $Cr^{3+}$ R-line fluorescence from sapphire and its application to crystal orientation and piezospectroscopic measurement. *J. Am. Ceram. Soc.*, 1997, **80**, 69–78.
20. Harlan, N. R., Merino, R. I., Peña, J. I., Larrea, A. and Orera, V. M., Phase distribution and residual stresses in melt-grown $Al_2O_3$–$ZrO_2(Y_2O_3)$ eutectics. *J. Am. Ceram. Soc.*, 2002, **85**, 2025–2032.
21. Dickey, E. C., Frazer, C. S., Watkins, T. R. and Hubbard, C. R., Residual stresses in high-temperature ceramic eutectics. *J. Europ. Ceram. Soc.*, 1999, **19**, 2503–2509.
22. *Annual Book of ASTM Standards*, 1999. Ed. American Society for Testing and Materials.
23. Lee, J. H., Yoshikawa, A., Durbin, S. D., Yoon, D. H., Fukuda, T. and Waku, Y., Microstructure of $Al_2O_3/ZrO_2$ eutectic fibres grown by the micro-pulling down method. *J. Cryst. Growth*, 2001, **222**, 791–796.
24. Echigoya, J., Takabayashi, Y. and Suto, H., Hardness and fracture toughness of directionally solidified $Al_2O_3$–$ZrO_2(Y_2O_3)$ eutectics. *J. Mater. Sci. Lett.*, 1986, **5**, 153–154.
25. Borodin, V. A., Starostin, M. Yu. and Yalovets, T. N., Structure and related mechanical properties of shaped eutectic $Al_2O_3$–$ZrO_2(Y_2O_3)$ composites. *J. Cryst. Growth*, 1990, **104**, 148–153.

26. Yang, J.-M., Jeng, S. M. and Chang, S., Fracture behavior of directionally solidified $Y_3Al_5O_{12}/Al_2O_3$ eutectic fiber. *J. Am. Ceram. Soc.*, 1996, **79**, 1218–1222.
27. Niihara, K., Morena, R. and Hasselman, D. P. H., Evaluation of KIC of brittle solids by the indentation method with low-crack-indent ratios. *J. Mater. Sci. Lett.*, 1982, **1**, 13–16.
28. Anstis, G. R., Chantikul, P., Lawn, B. R. and Marshall, D. B., A critical evaluation of indentation techniques for measuring fracture toughness: I. Direct crack measurements. *J. Am. Ceram. Soc.*, 1981, **64**, 533–538.
29. J.Y. Pastor, *private communication*.
30. Park, D. Y. and Yang, J. M., Effect of the microstructure on the mechanical properties of a directionally solidified $Y_3Al_5O_{12}/Al_2O_3$ eutectic fiber. *J. Mater. Sci.*, 2001, **36**, 5593–5601.
31. Ochiai, S., Ueda, T., Sato, K., Hojo, M., Waku, Y., Nakagawa, N., Sakata, S., Mitani, A. and Takahashi, T., Deformation and fracture behavior of an $Al_2O_3$/YAG composite from room temperature to 2023 K. *Compos. Sci. Technol.*, 2001, **61**, 2117–2128.